Effect of glycine molar ratios on structural and magnetic properties of combustion synthesized W-type Barium hexaferrites nanocrystalline

RAHIM SABBAGHIZADEH[a], ARMAN SEDGHI[b,*], ELHAM AMINI[b]

[a]Research and development Laboratory, Elite Lighting Company, 5430 Slauson Ave, Commerce, California, USA
[b]Materials Engineering Department, Imam Khomeini International University, Qazvin 34149-16818, Iran

Nanocrystalline $BaZn_{1.5}Co_{0.5}Fe_{16}O_{27}$ powders were fabricated via sol-gel combustion route and effect of the relative reductant-to-oxidant ratios (φ = 0.5, 1.0 and 15, respectively) of glycine fuel on characteristics of $BaZn_{1.5}Co_{0.5}Fe_{16}O_{27}$ nano ceramics were investigated. Thermodynamic modeling of the combustion reaction shows that by increasing the reductant-to-oxidant ratio, the amount of released gases and adiabatic flame temperatures will rise. The powders obtained by combustion were characterized by X-ray diffraction (XRD), Scanning electron microscopy (SEM) and vibrating sample magnetometer (VSM). Results showed that Samples are pure Ba-hexaferrite nano particles which their crystallite size was less than 87 nm.
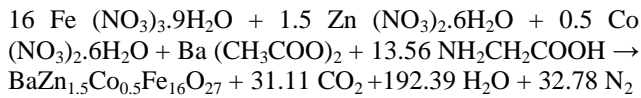
1. Introduction

Hexagonal ferrites are taking a lot of scientific interest by the researchers and scientists due to its various versatile properties such as superparamagnetic nature, quantum size and magnetic tunneling effect, larger surface to volume ratio, chemical stability, nontoxic behavior, easy to synthesize and moreover, applications in the field of energy and memory storage devices, permanent magnets, nanoelectronics, high density recording media, radar and communication system, biomedicine and water purification. [1,2]. There are six types of hexagonal ferrites such as M, W, Y, Z, X and U depending upon their crystal structure among which W-type hexaferrites having general formula BaMe2Fe16O27 or Co2W taking more attention because of its excellent magnetic properties as compared to other hexagonal ferrites [3]. Barium hexagonal ferrites have been widely used in magnetic recording, permanent magnets, microwave devices and electromagnetic shielding fields due to their high saturation magnetization, great coercivity, excellent chemical stability and corrosion resistance [4]. The W-type barium ferrite is used for electromagnetic wave absorber [5, 6] and radar absorbing materials due to their relative complex permeability, high magnetization, and planar anisotropic behavior [7]. The structural and magnetic properties of W-type hexagonal ferrite depend on many factors as like as synthesis method, sintering temperature, type, and amount of substitution [8–12]. Various methods have been proposed to synthesize nanocrystalline W-type hexagonal ferrite, such as the chemical co-precipitation, solid state oxide ceramic process, mechanical alloying, and sol–gel method [13-15].

However, these techniques usually include many sophisticated processes and consume much longer time. Moreover, they have not received much commercial attention due to lacking reproducibility, reliability, and cost effectiveness [16, 17, 18]. On the other hand, gel combustion, offer well-known advantages of liquid phase reactions with respect to solid phase reactions. In this method, dispersion of reactants takes place optimally, producing reactive samples which have low annealing or sintering temperature, and the distribution of the as-formed oxide components in the crystalline structure is uniform because of the precursor mixture homogeneity [19]. Among the various parameters such as the type and amount of the fuel, and the pH of the starting solution, fuel type plays an important role in determining the morphology, phase, and particulate properties of the final product. Glycine, one of the smallest amino acids with the formula NH_2CH_2COOH, is used as the reducing/complexing agent, the zwitterionic character of glycine can effectively complex various metal ions which help in preventing their selective precipitation and therefore in maintaining the compositional homogeneity among the constituents and it has high negative combustion heat (-3.24 kcal g^{-1}) as compared to urea (-2.98 kcal g^{-1}) and citric acid (-2.76 kcal g^{-1}) make a better exothermic reaction [20]. Several works were reported in the field of w-type Ba-hexaferrite powders preparation by gel combustion [21-24] but effect of fuel molar ratio on structural and magnetic properties of w-type Ba hexaferrites did not studied anymore. In this paper, effect of fuel to oxidizer ratio on formation of w-type Ba hexaferrites by gel combustion method, reaction
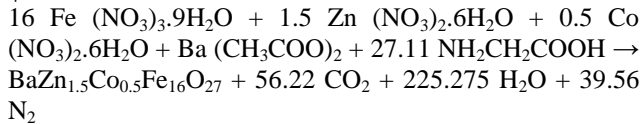
thermodynamics and structure and properties of reaction products were studied.
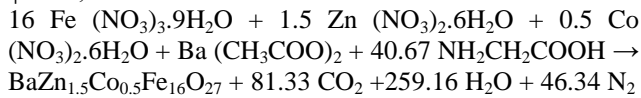
2. Experimental

Analytical grade, $Ba(CH_3COO)_2$, $Fe(NO_3)_3.9H_2O$, $Zn(NO_3)_2.6H_2O$ (all from Scharlau, Spain), $Co(NO_3)_2.H_2O$ (from Lach-ner, Czech Republic), glycine [$NH_2.CH_2.COOH$] (Scharlau, Spain) and ammonia (25 wt.% Merck, Germany) were used as raw materials. According to principle of propellant chemistry, the oxidizing and reducing valencies of various elements are taken as: C=4, H=1, O= -2, N=0, M=2,3, etc. Thus, total valencies of a divalent metal nitrate $M(NO_3)_2$ becomes −10; and that for trivalent metal nitrate $M(NO_3)_3$ becomes −15, Barium acetate and glycine will have the reducing valencies of +16 and +9 respectively. Hence to release maximum energy, the stoichiometric composition of redox mixture for the reaction requires -244+9m=0 or m=27.11 mol of glycine [20,25]. Thus in order to prepare $BaZn_{1.5}Co_{0.5}Fe_{16}O_{27}$, the reactants should be combined in a molar proportion of 1:1.5:0.5:16:27.11 for $Ba(CH_3COO)_2$:$Zn(NO_3)_2\cdot6H_2O$: $Co(NO_3)_2\cdot6H_2O$: $Fe(NO_3)_3\cdot9H_2O$: CH_2NH_2COOH respectively. Under equilibrium condition, combustion reactions can be expressed as follows:
φ = 0.5, fuel lean:

16 Fe $(NO_3)_3.9H_2O$ + 1.5 Zn $(NO_3)_2.6H_2O$ + 0.5 Co $(NO_3)_2.6H_2O$ + Ba $(CH_3COO)_2$ + 13.56 NH_2CH_2COOH → $BaZn_{1.5}Co_{0.5}Fe_{16}O_{27}$ + 31.11 CO_2 +192.39 H_2O + 32.78 N_2

φ = 1, stoichiometric:
16 Fe $(NO_3)_3.9H_2O$ + 1.5 Zn $(NO_3)_2.6H_2O$ + 0.5 Co $(NO_3)_2.6H_2O$ + Ba $(CH_3COO)_2$ + 27.11 NH_2CH_2COOH → $BaZn_{1.5}Co_{0.5}Fe_{16}O_{27}$ + 56.22 CO_2 + 225.275 H_2O + 39.56 N_2

φ =1.5, fuel rich:
16 Fe $(NO_3)_3.9H_2O$ + 1.5 Zn $(NO_3)_2.6H_2O$ + 0.5 Co $(NO_3)_2.6H_2O$ + Ba $(CH_3COO)_2$ + 40.67 NH_2CH_2COOH → $BaZn_{1.5}Co_{0.5}Fe_{16}O_{27}$ + 81.33 CO_2 +259.16 H_2O + 46.34 N_2

where φ is the multiplication factor, fuel lean means φ must be one, stoichiometric fuel means φ must be equal to one, and fuel rich condition means φ must be greater than one. For fabrication of samples, calculated amounts of barium acetate, ferric nitrate, cobalt nitrate, zinc nitrate were dissolved into 30 ml deionized water. Then the solution was magnetically stirred for 30 min, followed by certain amount of glycine addition. After that, ammonia was added into the solution to change the pH value from 1 to 4. Then solution was heated up to 80 °C to form the sol, then was heated up to 150 °C under constant stirring to transform sol into the viscous gel and gel was ignited and reacted in the air at 300 °C. As-burnt powder was calcined at 1050 °C for 2h.

The phase structure of powders was studied by X-ray diffraction (X– pert Philips Type: 3040/60 pw) in the range of 2θ=20°- 80°. The obtained peaks were compared with standard JCPDS cards No. 01-084-0927 and 01-078-1536 for determination of samples phase structure. The morphology of the powder was studied by scanning electron microscopy (SEM, Model: TESCAN-WEGA). The magnetic characterization of the powder was carried out by using vibrating sample magnetometer (VSM, Model: MDK daghigh kavir company, Iran) instrument. The crystallite size (D) of the powders was calculated by Debye–Scherrer's formula from X-ray diffraction curves of the samples:

$$D = \frac{0.9\,\lambda}{\beta\,cos\theta} \qquad (1)$$

where in equation 1, β is the broadening of the diffraction line measured at half maximum intensity (radians) and λ =1.5406Å, the wavelength of Cu-Kα and θ is the Bragg's angle. The lattice constants of the powder were calculated by using the following relationship:

$$\sin^2\theta = \frac{\lambda^2}{4}\left[\frac{4}{3}\times\frac{h^2 + hk + k^2}{a^2} + \frac{l^2}{c^2}\right] \qquad (2)$$

where in equation 2, (hkl) are Miller indices, and θ is the diffraction angle corresponding to the (hkl) plane.

3. Results and discussion

3.1. Nature of combustion reaction and thermodynamic analysis

To compare exothermicity of the various redox mixtures during combustion reactions, enthalpies of combustion and adiabatic flame temperature as a function of the fuel compositions were calculated. According to the thermodynamic data for the reactants and products listed in Table 1, the enthalpies of combustion reactions and the theoretical adiabatic flame temperature were approximately calculated by the following equation as a function of the reductant-to-oxidant ratio:

$$-\Delta H = \sum n\Delta H_p - \sum \Delta H_r = \int_{T_0}^{T_a}(\sum nCp)dT = -\int_{298}^{T_a}(\sum nCp)dT \qquad (3)$$

where ΔH_p and ΔH_r are the formation of the products and reactants, respectively, T_a is the theoretical adiabatic flame temperature, T_0 is the room temperature (298 K) and C_p is the molar heat capacity of products at constant pressure. It is worth noting that Cp is a function of temperature and, generally, it is usually expressed as $C_p = A + BT + CT^2 + DT^3$ (A, B, C and D are constants). However, the peak adiabatic flame temperature of the combustion is usually not too high, so ($CT^2 + DT^3$) has little influence on the calculated adiabatic flame temperature. Thus, C_p is nearly expressed as $C_p \approx A + BT$, as listed in Table 1, and used to calculate the adiabatic flame temperature.

Table 1. Thermodynamic data required for calculation of adiabatic flame temperature and enthalpy [26,27]

Compound	H°_f (kcal mol^{-1})	C_p (cal K^{-1} mol^{-1})
$Fe(NO_3)_3.9H_2O$(c)	-785.2	
$Zn(NO_3)_2.6H_2O$(c)	-551.3	
$Co(NO_3)_2.6H_2O$(c)	-528.49	
$Ba(CH_3Coo)_2$(c)	-354.79	
NH_2CH_2COOH(c)	-126.31	
$BaZn_{1.5}Co_{0.5}Fe_{16}O_{27}$ (c)[a]	-1860.93	$1038.9 - 0.0684T - 31636035.1/T^2$
H_2O(g)	-57.79	$7.2 + 0.0036T$
CO_2(g)	-94.05	$10.34 + 0.00274T$
O_2(g)	0	$5.92 + 0.00367T$
N_2(g)	0	$6.5 + 0.001T$

(c): crystalline; (g): gas; T: absolute temperature.
[a]Due to a lack of thermodynamic data for $BaZn_{1.5}Co_{0.5}Fe_{16}O_{27}$ (c), the enthalpy and specific heat of $SrFe_{12}O_{19}$ were used [27] because these two compounds are isostructure.

3.1.1. Enthalpies and adiabatic flame temperature of combustion

To investigate evolution of energy and flame temperature reached during combustion, the theoretical enthalpies of combustion and the theoretical adiabatic flame temperatures calculated according to the equation (3) as of the reductant-to-oxidant ratio are presented in Fig. 1.
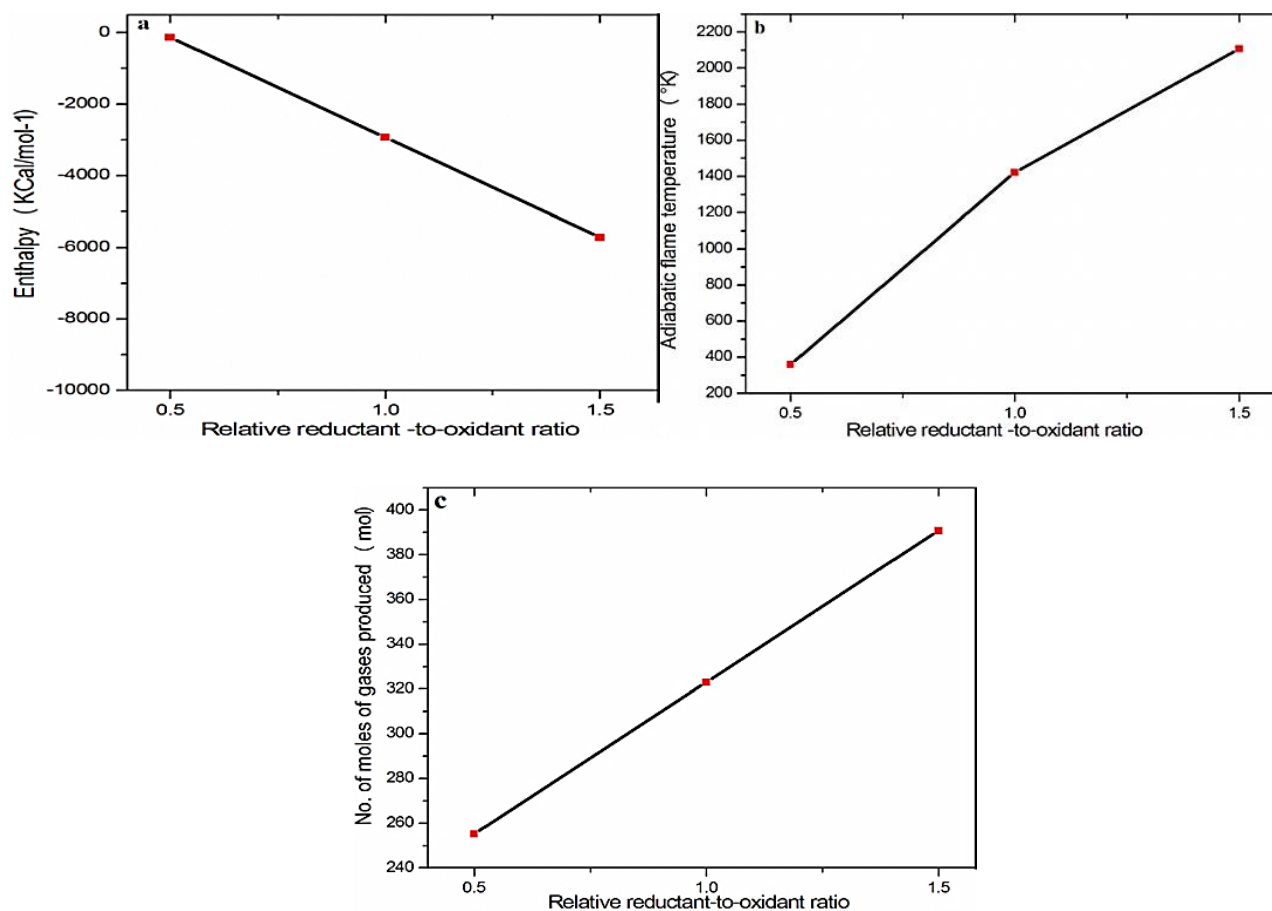

Fig. 1. (a)- The calculated enthalpies of various combustion reactions, (b)- The theoretical adiabatic flame temperature during combustion and (c)- Amount of gases produed during combustion, all of them as a function of the relative reductant-to-oxidant ratio

As expected, the calculated enthalpies, the theoretical adiabatic flame temperature of the combustion reactions and the number of moles gases produced during combustion are significantly increased as the relative reductant-to-oxidant ratio rises from 0.5 to 1.5. However, actual flame temperature is much lower than the theoretical value due to radiative losses, incomplete combustion, and convection losses through the atmosphere [28]. The powder characteristic, namely, crystallite size is primarily governed by enthalpy or flame temperature during combustion, where the flame temperature depends on nature of the fuel and its fuel molar ratio [29]. The amount of fuel is minimized in fuel lean system that leads to small amount of enthalpy, compared to the fuel rich and fuel stoichiometric systems. In fuel lean case there is more oxidant than reductant, φ it sets the system as an over-oxidizing state where, the excess oxygen would be heated and absorbed energy from reaction. Thus, the product temperature decreases from stoichiometric value, indicating the systems departure from equilibrium state [30,31]. Our results tend to indicate that glycine to nitrate molar ratio plays a predominant role for stoichiometric, fuel-lean and fuel-rich compositions.

3.2. X-ray diffraction analysis

Fig. 2 shows the XRD patterns of the three products synthesized by redox mixtures with φ equal to 0.5, 1.0 and 1.5, respectively. The obtained peaks are well matched with standard JCPDS cards No. 01-084-0927 and 01-078-1536. The well resolved broad diffraction peaks related to (110), (1010), (116), (204), (208), (2015), (2016), (306) and (220) reflection planes correspond to pure $BaZn_{1.5}Co_{0.5}Fe_{16}O_{27}$ phase with hexagonal structure the characteristic peaks become sharper and stronger as φ rises from 0.5 to 1.5, indicating that $BaZn_{1.5}Co_{0.5}Fe_{16}O_{27}$ crystalline are better crystallized and the nanocrystalline size which were calculated according to the Scherrer formula and listed in Table 2, is remarkably increased when the reductant-to-oxidant ratio (φ) increases. Weak diffraction peak corresponding to formation of α-Fe_2O_3 was observed in case of powder prepared by fuel lean condition (Fig. 2). This was since inadequate fuel could not react completely with metal nitrates to release enough heat to form well intermediate phases. XRD data enables to investigate the effect of ratio of fuel on structural parameters such as crystallite size (D) and lattice constants (a and c) for the $BaZn_{1.5}Co_{0.5}Fe_{16}O_{27}$ nanocrystallites. It can be seen from table that the value of D increases linearly with increase in reductant-to-oxidant ratio. The observed increase in crystallite size could be attributed to an increase in flam temperature which assists crystal growth [32].
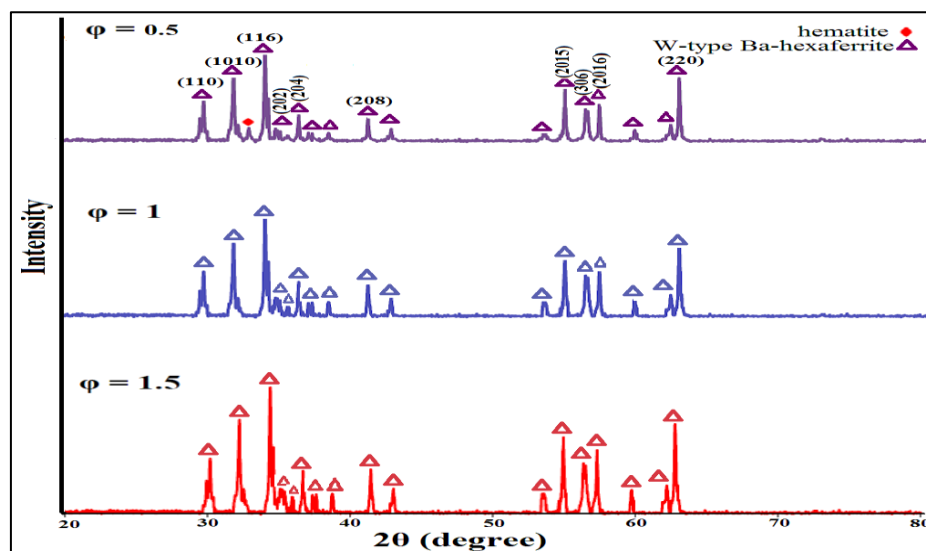

Fig. 2. XRD patterns of the sol-gel combustion synthesized products from the precursors with φ equal to 0.5, 1and 1.5, respectively

Table 2. The effect of reductant-to-oxidant ratio on crystallite size (D), lattice constant (a and c) of the $BaZn_{1.5}Co_{0.5}Fe_{16}O_{27}$powders

Multiplication factor (φ)	D(nm)	a(˚A)	c(˚A)	C.P[a]
0.5	48	0.585	3.287	BaZnCoW
1	51	0.589	3.311	BaZnCoW
1.5	87	0.599	3.526	BaZnCoW,α-Fe_2O_3,

[a]*Composition of Phases*

3.3. SEM analysis

Microstructures of the as-synthesized powders with different reductant -to-oxidant ratio are shown in Fig. 3. It is evident from images that agglomeration of crystallites is increased with fuel ratio.
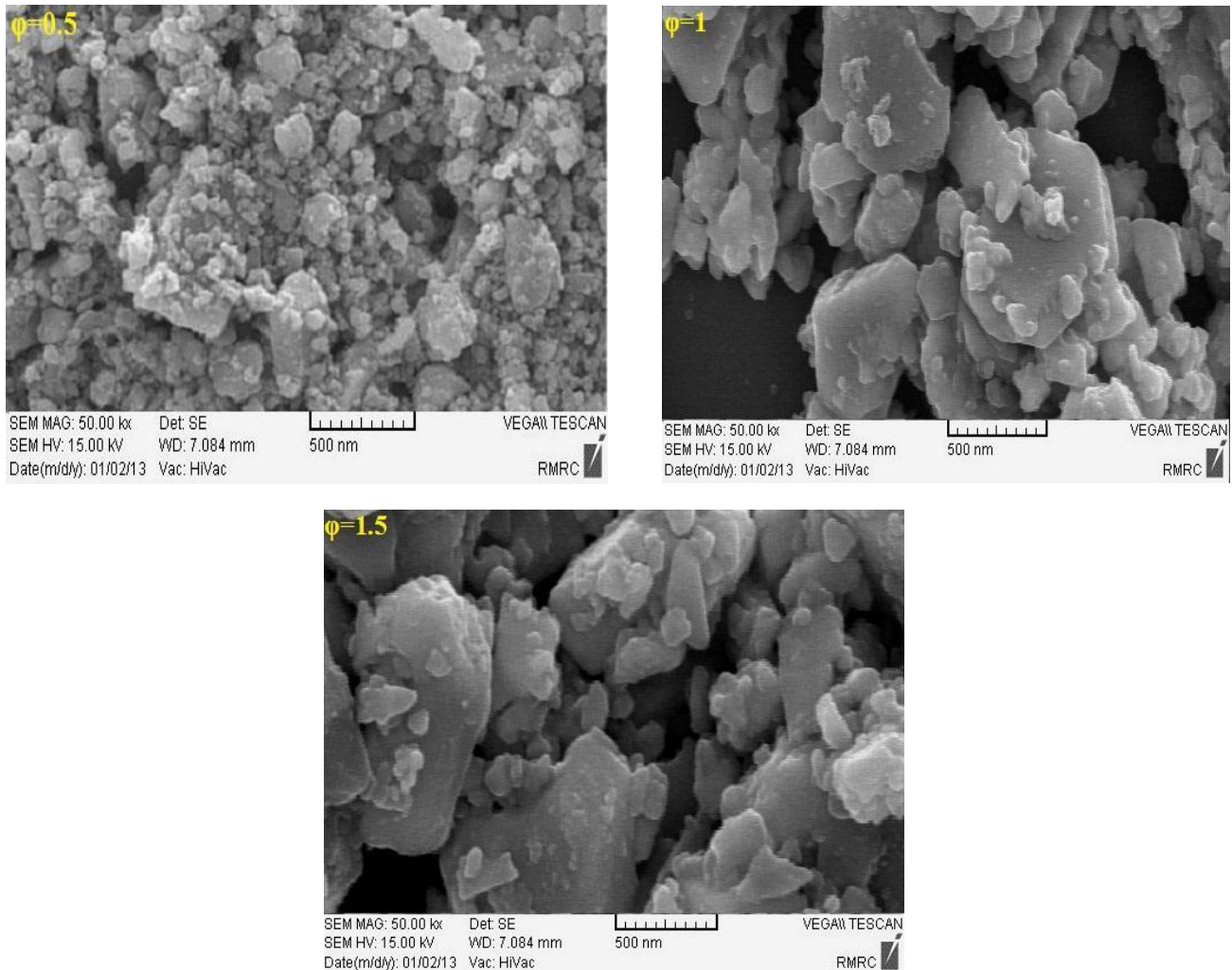

Fig. 3. Microstructures of the as-synthesized powders with different reductant -to-oxidant ratio φ=0.5, φ=1 and φ=1.5

As shown in Fig. 3, hard agglomerates of $BaZn_{1.5}Co_{0.5}Fe_{16}O_{27}$ nanocrystalline in the three powders were formed during combustion process. Furthermore, the agglomerates in the three powders are all submicron. Meanwhile, the degree of agglomeration of the powder φ = 1.5 appears to be larger than the samples were prepared by φ = 0.5 or φ = 1.0 ratios. It can be concluded that the morphology of the $BaZn_{1.5}Co_{0.5}Fe_{16}O_{27}$ nanocrystallite depends highly on amount of glycine added to initiate the combustion process. By increasing the amount of glycine in mixture, the flame temperature would increase and radical change in the microstructure was observed.

3.4. Magnetic properties

The hysteresis loops measured at room temperature for the $BaZn_{1.5}Co_{0.5}Fe_{16}O_{27}$ with different reductant-to-oxidant ratio are shown in Fig. 4. The S-shaped hysteresis loops of the powders show the behaviors of the soft magnets. The saturation magnetization (M_s) was very high, while coercive field (H_c) and remanent magnetization (M_r) were comparatively low, meaning that the powders exhibited quasi super paramagnetism. The M_s values are given in Table 3.
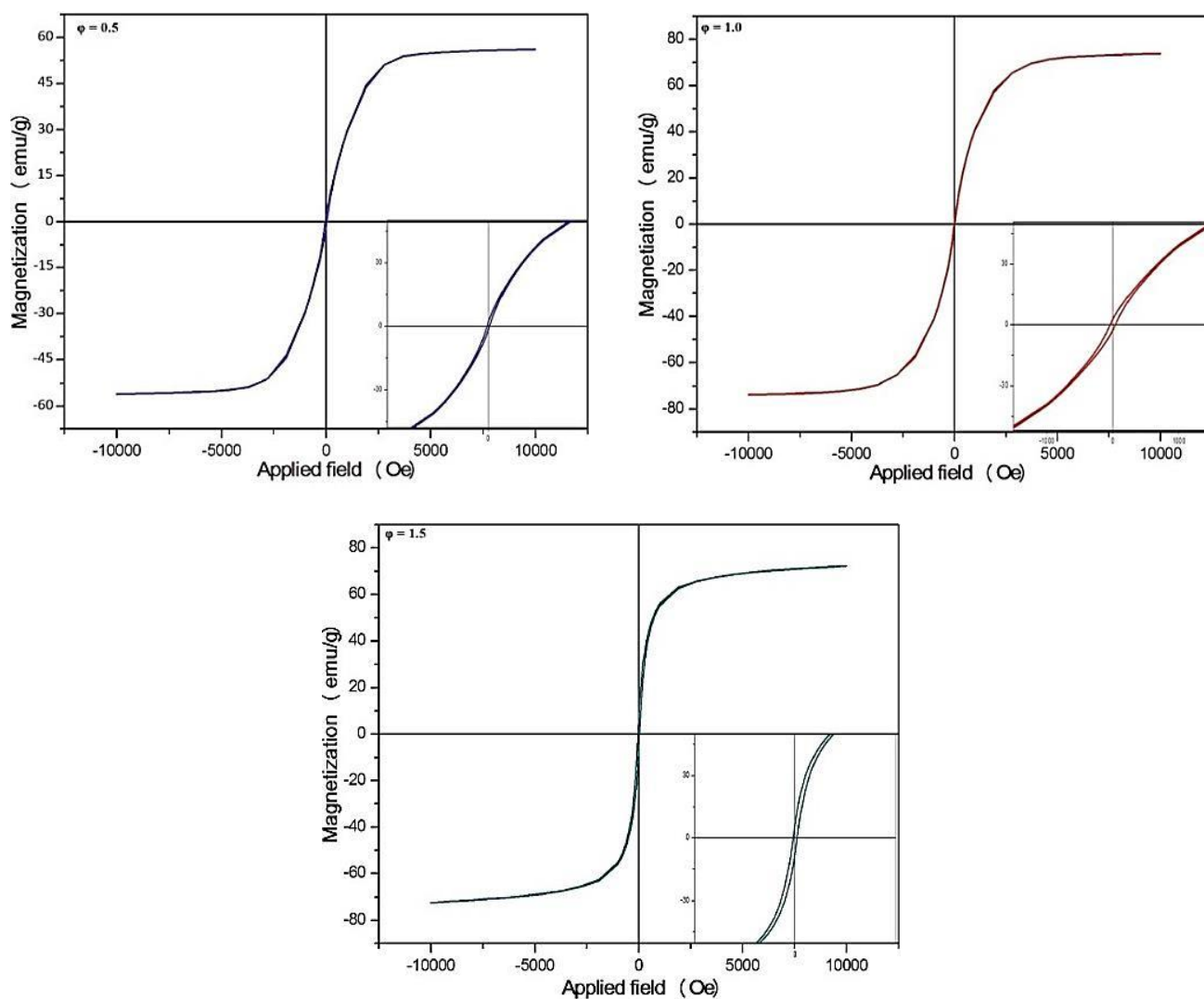
Fig. 4. Hysteresis loops of the powders with different reductant -to-oxidant ratio φ=0.5, φ=1 and φ=1.5

Table 3. Magnetic parameters of the $BaZn_{1.5}Co_{0.5}Fe_{16}O_{27}$ powders

Multiplication factor (φ)	Saturation magnetization, Ms (emu/g)	Remanence magnetization, M_r (emu/g)	Coercivity (Oe)
0.5	57.74	1.56	24.12
1	78.84	2.87	30.75
1.5	79.2	3.01	41.52

Both M_s and M_r would increase with the raising amount of fuel in combustion mixture. Crystallinity of powders was also found to increase with the raising amount of fuel in combustion mixture. The increasing of crystallinity will lead to burst increase in magnetization values. The low magnetization value (57.74 emu/g) is observed for fuel lean condition. The presence of canted anti-ferromagnetic α-Fe_2O_3, may contribute to the reduction in magnetization for fuel lean condition.

4. Conclusions

1. Thermodynamic consideration of the gel combustion formation of Nanocrystallite $BaZn_{1.5}Co_{0.5}Fe_{16}O_{27}$ powders by using glycine fuel shows that when reductant-to-oxidant ratio (φ) increases, the amount of gas produced and adiabatic flame temperature also increases. The much-pronounced effect was observed in cases of crystallite size, morphology, and magnetic properties of the products.
2. Study of samples with XRD, SEM and VSM was revealed that pure W-hexaferrite was formed but fabricated nanopowders were fully agglomerated and

samples gain better soft magnetic properties by changing fuel ratio.

3. It is observed that the lattice parameters and crystallite size are related to reductant-to-oxidant ratio (φ). As reductant-to-oxidant ratio (φ) increases, agglomeration increases due to hike in the flame temperature. Among the synthesized nanocrystallite $BaZn_{1.5}Co_{0.5}Fe_{16}O_{27}$ powders, the powder with $\varphi = 1$ show the high Saturation magnetization (M_s), low coercivity and small crystallite size as compared the power with $\varphi = 1.5$. This study concludes that, the fuel molar ratio plays a major role in deciding structural and magnetic properties of this hexaferrite.

References

[1] Rohit Jasrotia et al., Journal of Alloys and Compounds **830**, 154687 (2020).

[2] Kirti Singha et al., Journal of Sol-Gel Science and Technology **97**, 373 (2020).

[3] Rohit Jasrotia et al., AIP Conference Proceedings **2142**(1), AIP Publishing LLC, (2019).

[4] C. Sürig, K. A. Hempel, D. Bonnenberg, Applied Physics Letters **63**, 2836 (1993).

[5] N. K. Reddy, V. N. Mulay, Materials Chemistry and Physics **76**, 75 (2002).

[6] M. R. Meshram, N. K. Agrawal, B. Sinha, Journal of Magnetism and Magnetic Materials **271**, 207 (2004).

[7] Y. Yang, B. S. Zhang, W. D. Xu, Journal of Magnetism and Magnetic Materials **265**, 119 (2003).

[8] R. C. Puller, S. G. Appleton, A. K. Bhattacharya, Journal of Material Science Letter **17**, 973 (1998).

[9] E. M. Abo El Ata, M. A. Ahmed, Journal of Magnetism and Magnetic Materials **27**, 208 (2000).

[10] X. H. Wang, T. L. Ren, Y. Lil, Journal of Magnetism and Magnetic Materials **184**, 95 (1998).

[11] M. El-Saadawy, Journal of Magnetism and Magnetic Materials **219**, 69 (2000).

[12] S. P. Ruan, B. K. Xu, H. Suo, Journal of Magnetism and Magnetic Materials **212**, 175 (2000).

[13] Y. Zhang, H. T. Wang, J. W. Liu, Journal of New Chemistry Materials **36**, 63 (2008).

[14] L. Darja, Z. Andrej, S. Anna, Journal of the European Ceramic Society **28**, 2057 (2008).

[16] S. T. Aruna, Current Opinion in Solid State and Materials Science **12**, 40 (2008).

[17] K. C. Patil, S. T. Aruna, T. Mimani, Current Opinion in Solid State and Materials Science **6**, 507 (2002).

[18] R. Ianos, I. Lazau, Materials Chemistry and Physics **115**, 645 (2009).

[19] Z. Yue, J. Zhou, X. Wang, Z. Gui, L. Li, Journal of European Ceramic Society **23**, 189 (2003).

[20] A. F. Junior, T. E. P. Alves, E. C. De, O. Lima, E. Da, S. Nunes, V. Zapf, Applied Physics A **94**, 131 (2009).

[21] Y. Wu, Y. Huang, L. Niu, Y. Zhang, Y. Li, X. Wang, Journal of Magnetism and Magnetic Materials **324**, 616 (2012).

[22] J. Xu, H. Zou, H. Li, G. Li, S. Gan, G. Hong, Journal of Alloys and Compounds **490**, 552 (2010).

[23] L. Deng, L. Ding, K. Zhou, S. Huang, Z. Hu, B. Yang, Journal of Magnetism and Magnetic Materials **323**, 1895 (2011).

[24] M. Ahmad, I. Ali, F. Aen, M. U. Islama, M. N. Ashiq, Ceramics International **38**, 1267 (2012).

[25] S. R. Jain, K. C. Adiga, Combustion Flame **40**, 71 (1981).

[26] J. A. Dean (Ed.), Lange's Handbook of Chemistry, 15thed., McGraw-Hill, New York, 1998.

[27] S. K. Rakshit, S. C. Parida, S. Dash, Z. Singh, B. K. Sen, V. Venugopal, Journal of Solid-State Chemistry **180**, 523 (2007).

[28] R. D. Purohit, S. Saha, A. K. Tyagi, Journal of Nuclear Materials **288**, 7 (2001).

[29] L. E. Shea, J. McKittrick, O. A. Lopez, E. Sluzky, Journal of American Ceramic Society **79**, 3257 (1996).

[30] J. C. Toniolo, M. D. Lima, A. S. Takimi, C. P. Bergmann, Materials Research Bulletin **40**, 561 (2005).

[31] S. K. Sharma, S. S. Pitale, M. Malik, R. N. Dubey, M. S. Qureshi, S. Ojha, Physica B **405**, 866 (2010).

[32] N. M. Deraz, J. Anal. Appl. Pyrolysis **88**, 103 (2010).

*Corresponding author: sedghi@eng.ikiu.ac.ir